中國機械工程學刊第四十五卷第三期第 209~217 頁(民國一百一十三年)
Journal of the Chinese Society of Mechanical Engineers, Vol.45, No.3, pp209~217 (2024)

Copper-Reduction Alloy Design for Brake Pads

Tzung-Ming Chen* and Chung-Jia Huang**

Keywords：copper reduction, brake pads, powder metallurgy, alloy design.

ABSTRACT

In this study, a copper-reduction brake pad was designed based on environmental considerations. Solid diffusion calculations were performed for the brake pads containing 35 wt.% copper and 15 wt.% nickel. Functional alloy elements were added to the brake pads using a powder metallurgy process to achieve the desired results. The effect of each component on the mechanical properties of the pad was studied by adjusting the alloy ratio in the specimens. The binding behaviors of the copper substrate and additives were also analyzed. As a result, 35 wt.% copper and 15 wt.% nickel exhibited miscibility, and adding vanadium and silicon powder increased the bonding strength between the copper powder and the alloy. The maximum shear strength of the specimens reached 324 kgf, which is sufficient to cope with daily brake use. In addition, increasing the contents of tin, silicon, and nickel had a positive effect on the mechanical properties of the specimens with 35 wt.% copper, whereas, increasing the zinc content had a negative effect. Finally, the relationship among the copper concentration, sintering temperature, and time was calculated based on the diffusion theory, and the self-diffusion trend curves were plotted to obtain the sintering parameters so that the brake pad and the copper-sputtered back plate could reach 100% adhesion. Powder metallurgy related industries can reduce the number of trials in product development based on the results of this research, and can refer to the experimental parameters to plan the carbon-reduction process.

Paper Received February, 2024. Revised April, 2024. Accepted June, 2024. Author for Correspondence: Tzung-Ming Chen.
E-mail: tmchen@cc.ncue.edu.tw

* *Associate Professor, Department of Industrial Education and Technology, National Changhua University of Education, Changhua, Taiwan 50074, ROC.*

** *Graduate Student, Department of Industrial Education and Technology, National Changhua University of Education, Changhua, Taiwan 50074, ROC.*

INTRODUCTION

Dynamic equipment can be easily slowed down or stopped by bringing a brake disc and the moving part directly into contact. Kinetic energy is reduced by its conversion to friction heat. Disc-type brakes are widely used in bicycles and automobiles because of their high heat dissipation capability and stable braking effect (Day, 2014). In the previous decades, novel material formulations have been developed to meet the demands of greater braking force, safety, and environmental considerations. When asbestos was identified as a lung carcinogen, its use in brake disc formulations was banned. Thus, ceramics, Kevlar fiber, glass fiber, and graphite with similar strength and heat and fire resistance to those of asbestos were developed (Mahale et al., 2019). Brake pads contain various materials to meet the functional requirements, with each type having its advantages and limitations. For instance, metal-matrix composites can be used for high-speed trains. Carbon composites can be used for aircraft and formula race cars (Friedrich et al., 2015). Copper-based alloys are commonly applied in brake pads because of their excellent thermal conductivity and stable braking effect. Copper-based alloys can also be easily added to the formula in the form of substrates when applied to metal and semi-metal brake pads (Bijwe et al., 2018; Österle et al., 2010).

Particulate matter (PM) is commonly present in the atmosphere and has adverse effects on the environment and organisms (Arole et al., 2006). Motor vehicles are some of the major sources of PM. Vehicular PM can be divided into exhaust emissions and braking-induced emissions. Vehicle emission standards stipulated by governments have become increasingly strict. The development of electric vehicles is also encouraged to decrease exhaust PM emissions. Therefore, the PM caused by brake loss will be the focus of future improvement (Saha et al., 2023; Mulani et al., 2022; Denier van der Gon et al., 2013). As pointed out by many studies, the metal particles emitted by the brake pad wear process result in environmental deterioration (De Falco et al., 2023; Russo et al., 2023). For instance, these particles are partly responsible for the increase in the copper (Cu) concentration in the seawater of San Francisco Bay. This pollution harms salmon and other aquatic species (Sandahl et al., 2007). Therefore, Cu reduction is an important trend in brake-pad material development.

Here, a brake pad with a semi-metallic substrate was developed considering functionality, environmental protection, and low cost. Cu (35 wt.%) was chosen as the main component based on the diffusion calculations and experimental results. The proportions of other components were adjusted to test the material strength and braking effect. Furthermore, both of commercially available 60 wt.% Cu-based and a resin-based brake pads were compared with the new materials developed in this study. Finally, the relationship among the Cu concentration, diffusion temperature, and time was analyzed, and a set of sintering parameter curves were generated. In summary, the alloy of the low-cost Cu-reduction brake pad was designed by adjusting the composition ratio of the specimens and the sintering parameters.

METHODS

The semi-metallic brake pad specimens were made of 35 wt.% Cu as the main component, supplemented with friction modifiers, strengthening materials, and a solid lubricant. The sintering process parameters were selected based on the diffusion calculations. During liquid phase sintering a pressure continuously applied upon the specimens. After that, the hardness, shear strength, and braking force of the specimens were measured. Moreover, the composition was analyzed using an X-ray powder diffractometer, and the detected components were validated by diffusion computation. After identifying the effects of the additives on the brake-pad material, the composition was modified to obtain optimal shear strength, aiming to improve braking safety and strengthen the bond between the brake pad and the Cu-sputtered back plate.

FORMULATION

Fick's first law was used to calculate the diffusion behavior between the surface of the specimens that contained 45–25 wt.% Cu and the surface of the 99.9 wt.% Cu-sputtered back plate (Figure 1). The self-diffusion distance was set to 10,000 Cu atoms (approximately 2.56 μm). The calculation can be simplified to one-dimensional diffusion. The relationship among atomic concentration, diffusion time and distance after setting boundary conditions is shown in Equation (1):

$$C(x,t) - C_0 / C_S - C_0 = 1 - erf(x / 2\sqrt{Dt}) \quad (1)$$

where $C(x,t)$ represents the concentration of position x at time t, the common unit of time is seconds (s), and the unit of length is meters (m). C_S is the surface concentration; C_0 is the original atomic concentration in the material; D is the diffusion coefficient of the atom in the material (Smallman et al., 2014).

The calculation result showed that the self-diffusion with concentrations above 30 wt.% Cu reached more than 90 wt.% when the sintering temperature was 900 °C for 1 h. Thus, 35 wt.% Cu was selected as the base material as it provided a balance between the bonding strength and Cu content reduction. The remaining components of the specimen were chosen based on commercially available brake discs: components for solid lubrication, friction coefficient adjustment, dispersion strengthening, substrate strengthening, and a space filler. The materials selected for this study and their functional configurations are shown in Table 1.

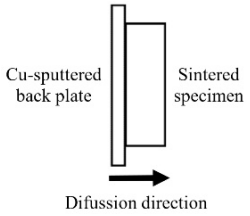

Fig. 1. Diagram of Cu self-diffusion direction.

Experiment

The wet powder-mixing method was used for a total amount of 20 g for each specimen. To prevent the demoulding failure, a small amount of white wax was added for internal lubrication (Huang et al., 2002). The powder was processed in a planetary mixer at 200 rpm for 4 h. The mixed powder was then heated in an oven at 60 ℃ for 1 h to remove water, and then the caked powder was removed using a 30-mesh screen. Before compression molding, a single 5 g raw billet was weighed with a precision balance, and 50 kgf was applied to compact the powder at room temperature under uniaxial pressure. Then, the raw billet was placed in a graphite mold with a load of 17 kgf, which was placed in a sintering furnace, and sealed around with a graphite ring (Figure 2). The specimens were sintered at 550 ℃ for 10 min and at 900 ℃ for 2 h. Finally, the sample was left to cool down in the furnace to room temperature and taken out.

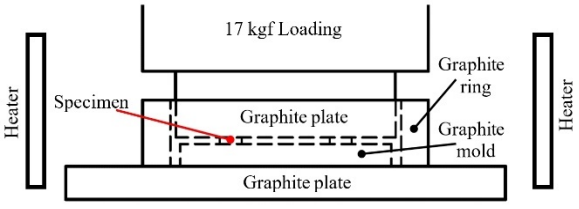

Fig. 2. Illustration of the sintering setup.

Table 1. Material-function configuration.

Substrate	Solid lubrication	Friction adjustment	Dispersion strengthening	Substrate strengthening	Space filling
Cu	Graphite	SiO_2	W/Mo/V/Si	Sn/Zn/Co/Ni	$BaSO_4$

Table 2. Elemental composition for the basic experiment.

Composition	Ni/Sn/Zn/Si/V/Graphite	Cu	Co	Mo	W	SiO_2	$BaSO_4$
%	Exploration	35	5	5	3	5	Bal.

Equipment

The Rockwell HRM hardness test was performed on a Mitutoyo AR-10 hardness tester, using a steel ball. The surface of the specimen was smoothed by a surface grinder before the test. The measurement points were around the center of the specimens. A shear test was conducted to install the clamp (Figure 3) in the universal test machine. Shear failure of the specimens were achieved by moving the slide block, and the machine was stopped immediately after the specimens were damaged. Finally, the failure strength of the specimens was analyzed through recording data, and the residual condition of the specimen on the back plate surface was inspected to identify the diffusion effect between the brake pad and the back plate. The braking force test was conducted according to DIN 79100. The brake disc was made of alloy-410 stainless steel. The specimen was placed in a caliper and ground against the disc. Dry and wet braking environments were tested with a running speed of 12.5 km/h. The braking time and release time were both 3 s and the gripping force was from 10 to 80 N. The brake was operated five times for every 10 N increase, and the braking force trend curve was used to judge whether the specimen met the specifications.

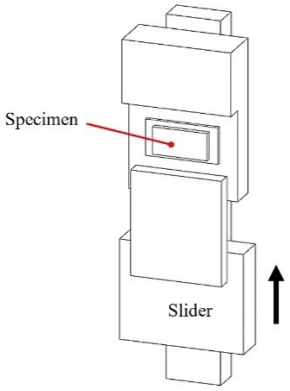

Fig. 3. Illustration of the shear test clamp.

RESULTS AND DISCUSSION

The effects of the component ratio on brake performance were analyzed. Based on the calculations using Fick's first law, 35 wt.% Cu powder was chosen as the substrate for the specimen. Cobalt (Co) powder was added at 5 wt.% as a strengthening element. Molybdenum (Mo) powder was added at 5 wt.% as a dispersion-strengthening element. Tungsten (W) powder was added at 3 wt.%. Moreover, the ratio of the friction coefficient-adjusting element (silicon dioxide, SiO_2) was 5 wt.%. Therefore, the substrate-strengthening elements (Ni, Sn, and Zn), the dispersion-strengthening elements (Si and V), and the ratio of the solid lubricant (graphite) are the main focus of the discussion. Barium sulfate ($BaSO_4$) was used as a space filler to ensure that the total composition ratio of each specimen was 100%. The component distributions are presented in Table 2.

Basic Formula

The effects of 0, 2, and 8 wt.% Sn on the mechanical properties of the specimens were compared at a fixed Zn concentration of 5 wt.%. The 5Zn0Sn specimen with 5 wt.% Zn and 0 wt.% Sn exhibited the highest hardness value (HRM 61), which was even higher than that of the commercial brake pad with 60 wt.% Cu (HRM 55). By contrast, the specimen prepared with 5 wt.% Zn combined with 2 wt.% Sn (i.e., 5Zn2Sn) and 5 wt.% Zn combined with 8 wt.% Sn (i.e., 5Zn8Sn) exhibited low hardness (HRM 26 and HRM 27, respectively) (Figure 4). Furthermore, the hardness of the specimen decreased with an increase in the amounts of Zn and Sn because these are soft materials. However, the hardness of $BaSO_4$ is higher than that of Zn and Sn. Thus, the hardness increased when the percentage of $BaSO_4$ was increased.

The alloy-410 stainless steel disc with a hardness of 60 HRC was selected as the grinding component in the experiment. If the hardness is too high, abnormal sound is produced during braking, and the braking disc may also be damaged, thus affecting the braking effect. The test results showed that the optimal shear strength of 5Zn8Sn was 210 kgf, which was approximately 25% higher than that of 5Zn2Sn (Fig. 4). However, the Sn content affected the strength of the specimen in the opposite way it affected hardness. Thus, increasing the percentage of Sn, which has low hardness but good bonding with the substrate, enhances the bonding strength of the specimen. In addition, the shear strength of 5Zn0Sn was 196 kgf, which was approximately 22.5% higher than that of

5Zn2Sn.

Specimens with a fixed Sn content of 8 wt.% and 6, 9, and 12 wt.% of Zn were tested to compare their mechanical properties. The results showed that 6Zn8Sn, 9Zn8Sn, and 12Zn8Sn were too weak to be measured, and the shear strengths of these specimens significantly decreased to 120, 92, and 82 kgf, respectively, as the Zn content increased. This result suggests that a higher Zn content results in a more pronounced weakening effect. This is because Zn and Sn are elements with low hardness. Moreover, the expansion coefficient of Zn (30.2 $\mu m \cdot m^{-1} \cdot K^{-1}$) destroyed the internal structure of the material during high-temperature sintering, resulting in weakening. This phenomenon is consistent with the results obtained by Chen et al. (2011) on the thermal expansion of a Cu-Zn alloy. The sintering temperature in the study was 900 °C, which was very close to the boiling point of Zn (907 °C). According to Koo et al. (2008) the post-sintering Zn content decreases as the sintering temperature decreases. Therefore, here, Zn likely vaporized from the substrate and formed holes, which lowered the density. This is directly related to the reduction in hardness. Our findings are consistent with the above-mentioned literature, confirming that increasing the Zn content leads to a reduction in both the hardness and shear strength of the specimen.

To confirm the effects on the mechanical properties of simultaneously lowering the Zn and Sn contents, two specimens (6Zn5Sn and 0Zn2Sn) were evaluated. As a result, 6Zn5Sn had a hardness of HRM 41 and its shear strength was 137 kgf. On the other hand, 0Zn2Sn had a hardness of HRM 57, and its shear strength was 152 kgf. In summary, 5Zn8Sn performed better and had a better base ratio than the other specimens.

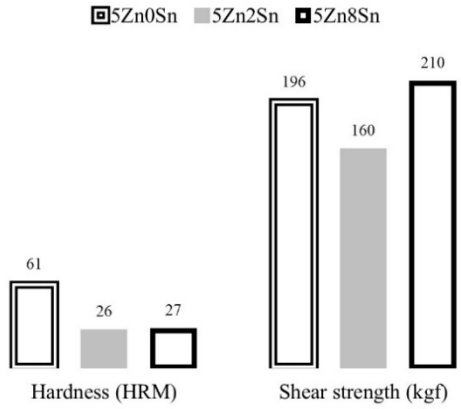

Fig. 4. Hardness and shear strength for specimens with three ratios of Zn and Sn.

Formula Improvement

V and Si were added to increase the strength of the base formula. The following four specimens were designed: 3V0Si, 6V0Si, 6V1.5Si, and 6V2Si. Their hardness values after sintering were HRM 47, HRM 30, HRM 42, and HRM 37, respectively. Their shear strengths were ranked as follows: 162 kgf for 3V0Si, 180 kgf for 6V0Si, 203 kgf for 6V1.5Si, and 225 kgf for 6V2Si (Figure 5). The test results revealed that 6 wt.% V combined with 1.5–2 wt.% Si enhanced the strength of the base formula.

Because of the solid-solution mechanism of Cu-Ni, although the thermal energy provided by the sintering furnace was not as high as that provided by the melting process, Ni and Cu both presented face-centered cubic lattice and their atomic radii differed by only 4 pm. Therefore, Ni was added to test its effect on the mechanical properties of the specimen. As a result, the hardness of 6V8.5Ni was HRM 33 and its shear strength was 171 kgf. The hardness of 6V10.5Ni was HRM 32 and its shear strength was 155 kgf. In addition, the hardness of 6V1Si15Ni was HRM 34 and its shear strength was 324 kgf (Fig. 5). Thus, adding Ni had no effect on the hardness of the specimen but contributed to its binding performance. For instance, the shear strength obtained with 15 wt.% Ni already exceeded that of commercially available resin-based brake pads and was sufficient to meet the actual braking requirements.

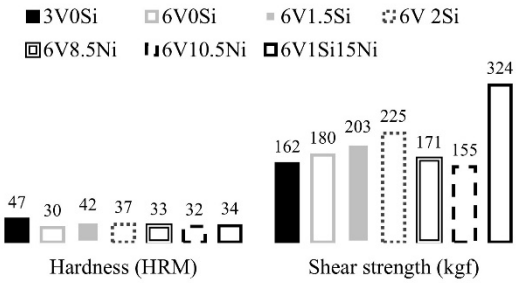

Fig. 5. Hardness and shear strength of six specimens containing V, Si, and Ni.

Strengthening Trends

After the base formula and the strengthening elements were selected, the effects of Ni, Si, Zn, and Sn on Cu-based substrate were evaluated. Ni, Si, and Sn enhanced the strength of the specimen. Nevertheless, a high Sn content affected the braking process, although it improved the strength of the substrate. Therefore, Sn can be added only in low amounts. Moreover, Zn weakened the specimen because of its high thermal expansion coefficient. The relationship between the content of each element and the shear strength of specimens is illustrated in Figure 6.

The Ni content is proportional to the strength of the specimen. To understand the solid-solution reaction of Cu-Ni after sintering, the 6V1Si15Ni and 5Zn8Sn specimens were analyzed using an X-ray diffraction (XRD) diffractometer. As a result, solid solutions of C, Cu, and Cu-Ni were detected in both specimens. Because the 6V1Si15Ni formula contained 15 wt.% Ni, whereas the 5Zn8Sn formula contained

only 5 wt.% Ni, the Cu_xNi_x peak of the 6V1Si15Ni specimen was stronger at 56° than that of the 5Zn8Sn specimen. Furthermore, increasing the Ni content was conducive to the formation of the Cu-Ni solid solution, which enhanced the strength of the substrate. In addition, the 5Zn8Sn specimen had a high Zn content; thus, a Cu_2Zn compound combined with Cu, as well as ZnS, was detected. By contrast, the 6V1Si15Ni formula had only 3 wt.% Zn; thus, its spectrum indicated only the presence of Zn. The results of the XRD analysis of 6V1Si15Ni and 5ZnSn are displayed in Figure 7.

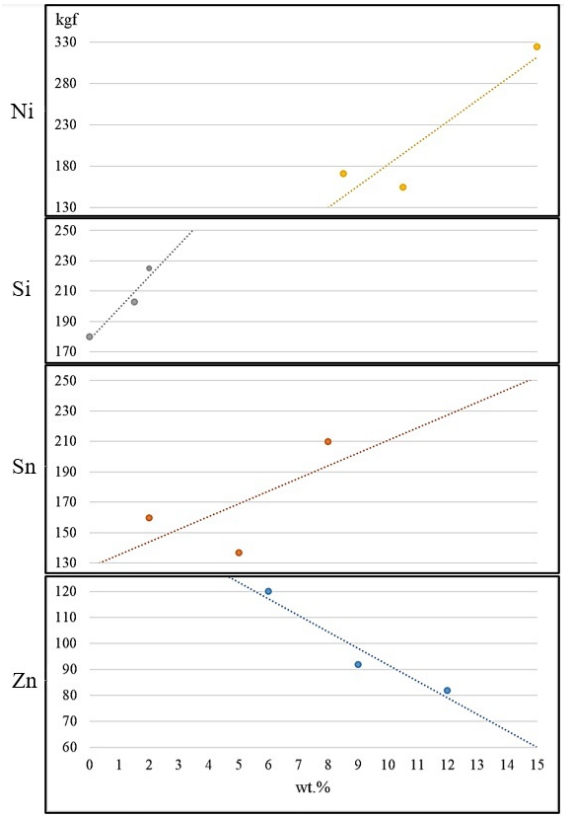

Fig. 6. Relationship between the Ni/Si/Sn/Zn content and shear strength of specimen.

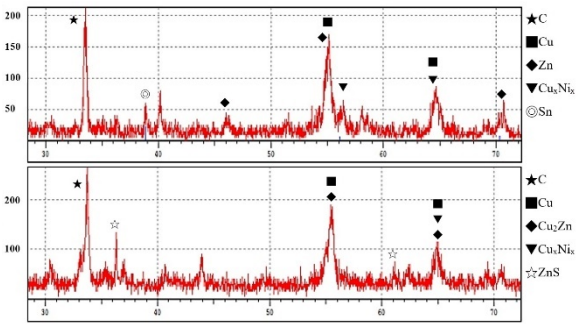

Fig. 7. XRD patterns of the specimens 6V1Si15Ni and 5ZnSn.

Friction Adjustment

The lubrication effect of graphite in the braking process can be used to adjust the friction coefficient of the brake pad. To understand the effect of graphite addition on the hardness and shear strength of the specimens, 3, 6, and 9 wt.% graphite was added to the basic formula of 5Zn8Sn. The test results showed that the hardness and shear strength of the specimen decreased with an increase in the graphite content. The hardness and shear strength of 5Zn8Sn3G were HRM 67 and 141 kgf, respectively, whereas, the hardness and shear strength of 5Zn8Sn6G were HRM 48 and 111 kgf, respectively (Figure 8). The surface of the 5Zn8Sn9G specimen was severely damaged during mechanical grinding, indicating insufficient material strength, so subsequent hardness and shear strength tests could not be performed. The results revealed that a graphite concentration of 3–5 wt.% was suitable.

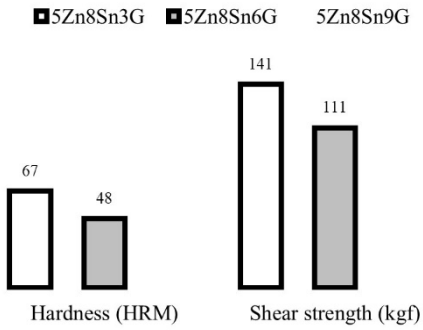

Fig. 8. Hardness and shear strength of three groups of graphite-added specimens.

Braking Force Test

The braking force is a major factor to consider when choosing a brake pad. When the braking effect is too high or too low, driving safety is endangered. Thus, a braking force test was carried out in both dry and wet environments. The grip force was 80 N. The measured braking force was divided into three categories: failure (NG), medium (M), and excellent (E). The effect of each component percentage on the braking force was analyzed. The braking force test was carried out only for the braking pads that had a shear strength greater than 180 kgf because specimens with insufficient strength cracked during the test and resulted in inaccurate data.

The test results showed that 5Zn8Sn and 5Zn0Sn belong to the NG category. The reason behind the failure of 5Zn8Sn was the excessive Sn content. During the braking test with a 60 N grip force, the temperature of the brake disc was approximately 450 °C, which is higher than the melting point of Sn. Therefore, the material experienced softening and the braking force did not improve for a 60–80 N grip force. Hence, the specimen failed. 5Zn0Sn failed because of material rupture during the test as a result of the excessive content of Zn. Although the shear strength reached 196 kgf after sintering, the high temperature

during the braking process caused the Zn inside the material to expand, resulting in material rupture. In addition, the test results of 5Zn8Sn and 5Zn0Sn confirmed the negative braking effects of Zn and Sn when their contents exceeded 5 wt.%. Although the braking force of other specimens did not reach the level of performance of the two groups of commercial brake pads, all the specimens met the requirements of DIN 79100, suggesting that they could pass the braking test when subjected to a shear strength higher than 180 kgf. Moreover, adding a small amount of high-hardness material is a feasible approach for improving the braking force effect without affecting the strength of the material or damaging the braking disc. The results of the braking force test are presented in Table 3.

Table 3. Results of the braking force test.

Specimen	Shear strength (kgf)	Dry	Wet
5Zn8Sn	210	NG	NG
5Zn0Sn	196	NG	NG
6V0Si	180	M	M
6V1.5Si	203	M	M
6V2Si	225	M	M
15Ni	324	M	M
60Cu	528	E	E
Resin	317	E	E

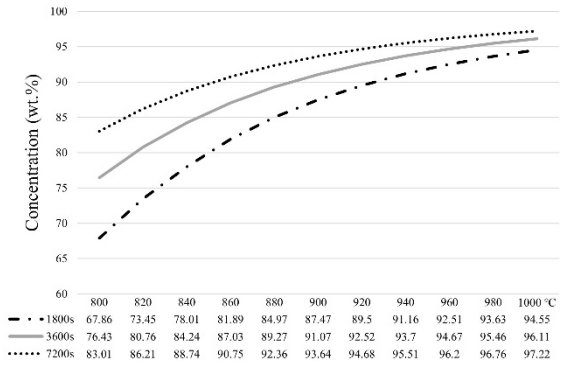

Fig. 9. Relationship between the self-diffusion concentration of Cu and the temperature at a fixed diffusion distance.

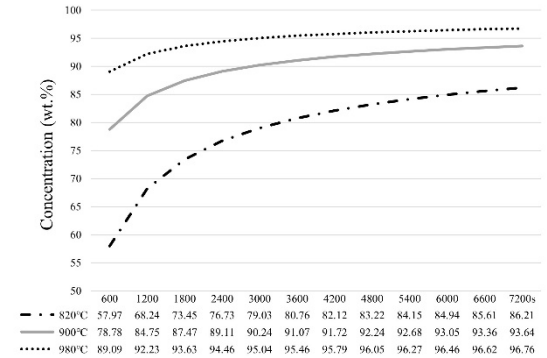

Fig. 10. Relationship between the self-diffusion concentration of Cu and the time at a fixed diffusion distance.

Diffusion Behavior

For safety reasons, the brake pad was combined with a Cu-sputtered back plate during sintering to increase strength and prevent corner breakage. To understand the influence of the sintering parameters on the self-diffusion behavior of Cu, Fick's first law was used to calculate four conditions. Then, three groups of parameters were selected for sintering. Finally, a shear failure test was carried out to determine the area of the residual specimen on the back plate surface and validate the calculation results. The Cu concentration on the back plate surface was set at 99.9 wt.% for all four calculations. For the first two conditions, the diffusion distance was set at a diameter of 10,000 Cu atoms (~2.56 μm). The change in the concentration at a given position was calculated using different sintering temperatures and durations (Figures 9 and 10). For the remaining two conditions, a specific position with a Cu self-diffusion concentration of 90 wt.% was set, and the distance from that location to the back plate was calculated at different sintering temperatures and durations (Figures 11 and 12).

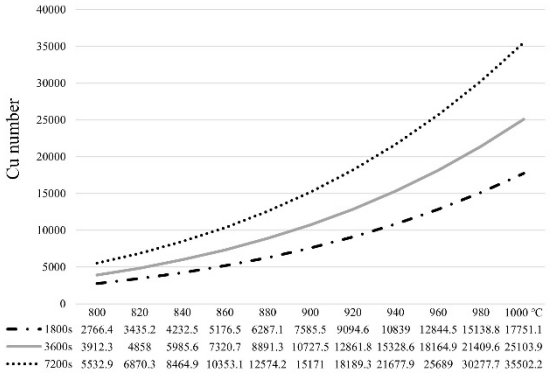

Fig. 11. Relationship between the self-diffusion distance of Cu and the temperature at a fixed diffusion concentration.

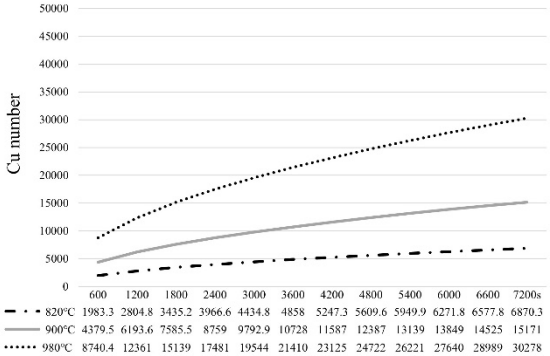

Fig. 12. Relationship between the self-diffusion distance of Cu and the time at a fixed diffusion concentration.

The calculations revealed that increasing the sintering

temperature had a significant positive effect on the self-diffusion of Cu. For example, the self-diffusion concentration reached 86.21 wt.% after the specimen was continuously sintered at 820 ℃ for 7200 s. However, the self-diffusion concentration reached 87.47 wt.% when the specimen was continuously sintered at 900 ℃ for 1800 s. This results in major time and cost advantages (Fig. 10). When the sintering temperature increased, the distance from the position corresponding to the 90 wt.% concentration to the back plate increased after diffusion. With a fixed sintering duration of 1800 s, the difference between the sintering temperatures of 820 ℃ and 900 ℃ represented 4150.3 times the Cu atom diameter (~1.06 μm) (Fig. 12). The calculations also revealed that when the self-diffusion concentration exceeded 90 wt.%, the increase in concentration gradually slows down (Fig. 10). Moreover, from 600 to 3600 s, the self-diffusion concentrations for the three sintering temperatures increased by 22.85, 12.29, and 6.37 wt.%. However, from 3600 to 7200 s, the increase was only 5.47, 2.57, and 1.3 wt.%. Although continuous sintering at 980 ℃ for 7200 s resulted in the best diffusion effect, it was time-consuming and increased the cost of equipment maintenance.

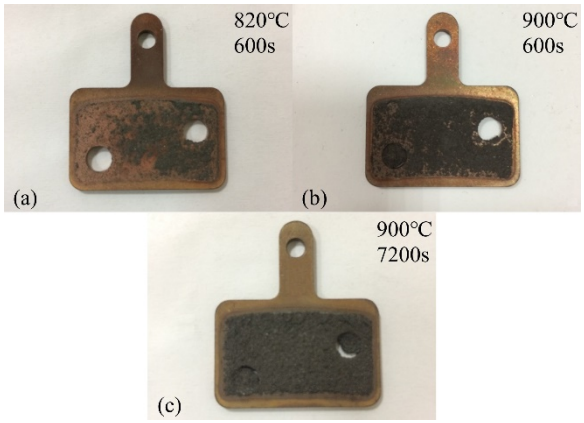

Fig. 13. Surface of the back plate after sintering: (a) the first group of specimens; (b) the second group of specimens; (c) the third group of specimens.

To compare the results of the calculations versus the actual test data of sintering, the 6V1Si15Ni specimens were sintered at three temperatures. The first group was continuously sintered at 820 ℃ for 600 s, the second group was continuously sintered at 900 ℃ for 600 s, and the third group was continuously sintered at 900 ℃ for 7200 s. The shear failure test was conducted after sintering to observe residual brake pieces on the back plate surface. As shown in Figure 13, the first group of brake pads exhibited poor diffusion performance, and only a small part of the material was combined with the back plate. This condition may result in the brake pad separating from the back plate during braking and is a risk factor for accidents. In addition, the adhesion area in the second group of brake pads did not reach 100%. Therefore, increasing the sintering temperature can strengthen the bonding. The adhesion area of the third group reached 100%, indicating that extending the sintering duration improved the diffusion effect and the test result was consistent with the calculated diffusion.

CONCLUSIONS

Different test pads with different composition ratios were fabricated and tested to understand their strengthening mechanism. The sintering parameters of the brake pads were calculated using Fick's first law to reduce the amount of Cu used. The main conclusions of this study are as follows:

1. Sn, V, Si, and Ni at the weight percentages used in this study increased the shear strength of the specimens. The shear strength reached 200 kgf when 6 wt.% V and 1.5 wt.% Si was added, indicating a slight improvement in the binding effect between the materials. However, a content of Zn over 5 wt.% lowered the shear strength. The brake test also showed a negative effect when the Sn content was greater than 8 wt.%. Therefore, only a small amount of Zn or Sn can be added to the brake pads.
2. When Ni was increased to 15 wt.%, the shear strength increased to 324 kgf, which is higher than that of commercially available resin-based brake pads. Hence, the best interface-binding effect was attained when 15 wt.% Ni and 35 wt.% Cu was used. The XRD analysis confirmed that the Cu-Ni solution was the main factor behind the strengthening of the substrate.
3. The self-diffusion trend of Cu was calculated using Fick's first law to understand the relationship among the substrate concentration, sintering temperature and time. The test result revealed that the adhesion of the sintered specimen to the Cu-sputtered back plate surface was consistent with the calculated results. Thus, when the substrate percentage is adjusted for different applications, the calculation can quickly predict the result and substantially reduce the testing time. Therefore, this practice provides a useful guide for designing powder metallurgy processes.

The development of environmentally friendly brake pads has become the focus of related industries in recent years because of the increasingly stricter environmental protection regulations. Although the optimal formula presented in this study enhances the bonding effect between the materials, the reduction of the Cu content is still the main direction of future research. The friction coefficient and wear rate of the materials can be optimized to balance braking performance and service life. Because Cu is an effective heat dissipator, a decrease in the Cu content leads to lowered heat transfer performance. Therefore, adding appropriate heat dissipation components is also

an attractive research direction.

ACKNOWLEDGEMENTS

The authors thank Tektro Technology Corporation for providing experimental equipment, consumables, and research funding.

REFERENCES

Arole, K., Velhal, M., Tajedini, M., Xavier, P.G., Bardasz, E., Green, M.J. and Liang, H., "Impacts of particles released from vehicles on environment and health," Tribology International, Vol.184, 108417 (2006).

Bijwe, J., Kumar, M., Gurunath, P.V., Desplanques, Y. and Degallaix, G., "Optimization of brass contents for best combination of tribo-performance and thermal conductivity of non-asbestos organic (NAO) friction composites," Wear, Vol.256, pp.699-712 (2008).

Chen, Y., Liu, L., Wang, Y., Liu, J. and Zhang, R., "Microstructure evolution and thermal expansion of Cu-Zn alloy after high pressure heat treatment," Transactions of Nonferrous Metals Society of China, Vol.21, pp.2205-2209 (2011).

Day, A.J., Braking of Road Vehicles, Elsevier, New York, pp.9-34 (2014).

De Falco, G., Russo, G., Ferrara, S., De Soccio, V., D'Anna, A., "Sustainable design of low-emission brake pads for railway vehicles: An experimental characterization," Atmospheric Environment: X, Vol.18, 100215 (2023).

Denier van der Gon, H.A.C., Gerlofs-Nijland, M.E., Gehrig, R., Gustafsson, M., Janssen, N., Harrison, R.M., Hulskotte, J., Johansson, C., Jozwicka, M., Keuken, M., Krijgsheld, K., Ntziachristos, L., Riediker, M. and Cassee, F.R., "The policy relevance of wear emissions from road transport, now and in the future — An international workshop report and consensus statement," Journal of the Air & Waste Management Association, Vol.63, pp.136-149 (2013).

Friedrich, K. and Breuer, U., Multifunctionality of Polymer Composites, Elsevier, Wood Dale, pp.551-572 (2015).

Huang, H.S., Lin, Y.C. and Hwang, K.S., "Effect of lubricant addition on the powder properties and compacting performance of spray-dried molybdenum powders," International Journal of Refractory Metals & Hard Materials, Vol.20, pp.175-180 (2002).

Koo, J., Araki, H. and Jung, S., "Effect of Zn addition on mechanical properties of brass hollow spheres," Materials Science and Engineering: A, Vol.483-484, pp254-257 (2008).

Mahale, V., Bijwe, J. and Sinha, S., "Efforts towards green friction materials," Tribology International, Vol.136, pp.196-206 (2019).

Mulani, S.M., Kumar, A., Shaikh, H.N.E.A., Saurabh, A., Singh, P.K. and Verma, P.C., "A review on recent development and challenges in automotive brake pad-disc system," Materials Today: Proceedings, Vol.56, pp.447-454 (2022).

Österle, W., Prietzel, C., Kloß, H. and Dmitriev, A.I., "On the role of copper in brake friction materials," Tribology International, Vol.43, pp.2317-2326 (2010).

Russo, C., Gautier di Confiengo, G., Magnacca, G., Faga, M.G. and Apicella, B., "Insights on non-exhaust emissions: An approach for the chemical characterization of debris generated during braking," Heliyon, Vol.9, e20672 (2023).

Saha, D., Sharma, D. and Satapathy, B.K., "Challenges pertaining to particulate matter emission of toxic formulations and prospects on using green ingredients for sustainable eco-friendly automotive brake composites," Sustainable Materials and Technologies, Vol.37, e00680 (2023).

Sandahl, J.F., Baldwin, D.H., Jenkins, J.J. and Scholz, N.L., "A Sensory System at the Interface between Urban Stormwater Runoff and Salmon Survival," Environmental Science & Technology, Vol.41, pp.2998-3004 (2007).

Smallman, R.E. and Ngan, A.H.W., Modern Physical Metallurgy, Elsevier, Waltham, pp.287-316 (2014).

減銅煞車片之合金設計

陳宗明　黃重嘉
國立彰化師範大學工業教育與技術學系

摘 要

本研究以環保考量為前提進行半金屬基煞車片之減銅合金設計。經過固體擴散計算以 35 wt.% 銅含量加上 15 wt.% 鎳含量為基礎，透過粉末冶金製程可將功能性合金元素加入煞車片並達到預期成效。研究過程調整合金比例以探討各成分含量對 35 wt.% 含銅煞車片機械性質的影響，並分析銅基材與添加材料之結合行為。研究成果顯示 35 wt.% 銅含量與 15 wt.% 鎳含量之固溶效果明顯，而添加釩和矽粉末可以提升銅粉末與合金之間的結合強度而使試片之剪力強度達 324 kgf，足以應付日常制動使用。另外，在實驗設定範圍內增加錫、矽和鎳三種元素的含量與 35 wt.%含銅試片機械性質之

強化有正向關係，但鋅含量增加則有負面效應。最後以擴散理論計算銅元素之濃度、燒結溫度和時間三者之間的關係，並建立自體擴散趨勢曲線以便掌握燒結參數，使煞車片與鍍銅背板達到 100%結合。未冶金相關產業可依據本研究成果減少產品開發之試作次數，更可參考各實驗參數以規劃減碳製程。